Article

Structural and Physicochemical Characterization of Chitosan Obtained by UAE and Its Effect on the Growth Inhibition of *Pythium ultimum*

Héctor Martín-López [1], **Soledad Cecilia Pech-Cohuo** [1], **Emanuel Herrera-Pool** [1],
Nelly Medina-Torres [1], **Juan Carlos Cuevas-Bernardino** [2], **Teresa Ayora-Talavera** [1],
Hugo Espinosa-Andrews [3], **Ana Ramos-Díaz** [1], **Stéphane Trombotto** [4] and **Neith Pacheco** [1,*]

1 Center for Research and Assistance in Technology and Designo f the State of Jalisco, AC Centro de, CIATEJ Southeast Unit, Parque Científico Tecnológico de Yucatán, Km 5.5. Carretera Sierra Papacal—Chuburná Puerto, Mérida, Yucatán 97302, Mexico; hemartin_al@ciatej.edu.mx (H.M.-L.); spech_al@ciatej.edu.mx (S.C.P.-C.); ivherrera_al@ciatej.edu.mx (E.H.-P.); arapachecol@gmail.com (N.M.-T.); tayora@ciatej.mx (T.A.-T.); aramos@ciatej.mx (A.R.-D.)

2 CONACYT—Center for Research and Assistance in Technology and Designo f the State of Jalisco, AC, Southeast Unit, Parque Científico Tecnológico de Yucatán, Km 5.5. Carretera Sierra Papacal—Chuburná Puerto, Mérida, Yucatán 97302, Mexico; jcuevas@ciatej.mx

3 CIATEJ Zapopan Unit, Camino Arenero 1227, El Bajío del Arenal, 45019 Zapopan Jalisco, Mexico; hespinosa@ciatej.mx

4 Ingénierie des Matériaux Polymères (IMP), CNRS UMR 5223, Université Claude Bernard Lyon 1, Univ Lyon, Villeurbanne F-69622, France; stephane.trombotto@univ-lyon1.fr

* Correspondence: npacheco@ciatej.mx

Abstract: The objective of this work was the recovery of chitosan by ultrasound-assisted extraction (UAE) from white shrimp (*Litopenaeus vannamei*) chitin, and the physicochemical and structural characterization of the obtained biopolymer, as well as its antimicrobial effect on *Pythium ultimum* growth. A 2^3 factorial design was used to evaluate chitosan extraction conditions. Instrumental analysis techniques for chitosan characterization and radial growth inhibition, as an antifungal activity test, were performed. The ultrasonically extracted chitosan (UC) reached a yield of 86.96% with 100% solubility, a degree of deacetylation (DDA) >78%, molecular weight (M_W) of 3.928×10^5 g mol^{-1}, and a crystallinity index (*Icr*) of 87%, calculated through nuclear magnetic resonance (^{1}H NMR) and Fourier transform infrared spectroscopy (FTIR), size exclusion chromatography (SEC), and X-ray diffraction (XRD), respectively. The inhibitory activity of the chitosan was evaluated against the oomycete *Pythium ultimum*, observing a 93% radial inhibition over 24 h. UAE proved to be an excellent alternative to the conventional deacetylation, reducing reaction time and obtaining a UC with higher M_W and (*Icr*) than the commercial one, which could potentiate its applications.

Keywords: antimicrobial activity; chitosan; deacetylation; *Litopenaeus vannamei*; Pythium ultimum; ultrasound-assisted extraction

1. Introduction

Chitin is a structural biopolymer with an analogous function to collagen in higher animals and cellulose in plants, and is mainly isolated from the exoskeletons of crustaceans, particularly shrimp waste [1,2]. Chitosan, the deacetylated derivative of chitin, is a polysaccharide composed of β-1,4-linked 2-acetamido-D-glucose and β-1,4-linked 2-amino-D-glucose units, where the chitin acetyl groups are substituted by amino groups on the C-2 position in the carbon chain [3,4]. Chitosan deacetylation can

be carried out by a chemical method that employs concentrated alkaline solutions for long periods, causing structural modifications in the resulting chitosan [4,5]. A biological method is also available, that allows a reduction in the degree of depolymerization due to greater control of the process; however, the use of chitin-deacetylase makes it a high-cost and low-yield process [5]. Due to limitations in these procedures, several studies have evaluated the implementation of complementary technologies, such as; a freeze-pump out-haw cycle [5], gamma irradiation [6], microwaves [7], and ultrasound [8], the latter being a simple, viable, and environmentally friendly technology [8,9]. Several studies have reported the application of ultrasound during chitin deacetylation from giant shrimp (*Macrobachium rosenbergii*), white shrimp (*Litopenaeus vannamei*), shrimp waste (*Parapenaeus longirostris*), and squid pen (*Teuthis spp.*) residues, demonstrating that ultrasound technology is an efficient method, thanks to the cavitation effect [8–10]. On the other hand, due to its biodegradability, biocompatibility, and non-toxicity, chitosan is considered an affordable, readily available, renewable, and sustainable material that exhibits different industrial applications in areas like drug delivery systems, water treatment, the manufacture of textiles, cosmetics, pharmaceutics, and biomedicine [3,4,11]. The biological, functional, and physicochemical properties of chitosan are closely related to the degree of deacetylation (DDA) or degree of acetylation (DA), and molecular weight (M_W), parameters that directly influence its pKa, viscosity, gelling capacity, and solubility [4,12]. To determine the DDA in chitosan, specific bands of functional groups obtained by Fourier transform infrared spectroscopy (FTIR) [13], and the ^{1}H NMR spectrum were employed to analyze this parameter [14]. It has been reported that high M_W and low DA values are associated with an improvement in antimicrobial activity [15]. Chitosan with a lower DA exhibits higher antimicrobial activity, due to a high positive charge that allows chitosan to dilute in acidified media [16,17]. Meanwhile, M_W influences the flexibility of the functional groups that interact with the microbial cells [18]. Furthermore, the crystallinity determined by X-ray diffraction (XRD) is related to the antimicrobial activity of chitosan, because the molecular arrangements in the structure of the polysaccharide may generate an electrostatic interaction with the microbial cell walls [19]. Chitosan antimicrobial activity has been well documented against bacterial strains and phytopathogenic fungi [20,21]. Nevertheless, few studies have been reported against oomycetes (diploid microorganisms capable of forming mycelium and sporangia) [22,23]. The Oomycetes genus *Pythium* are microorganisms capable of infecting a wide variety of plant species, affecting the yield and quality of agricultural products such as soybean, maize, wheat, rye, and canola, resulting in economic losses [23,24]. *Pythium ultimum,* characterized as being a saprotrophic phytopathogen, is capable of producing oospores that survive for long periods, infecting seeds and roots, but also inducing the necrosis of its host to feed [23,25]. The typical treatment for the control of these phytopathogens involves the use of synthetic pesticides; however, these agents are proven to be harmful to the environment, and can remain active in the water, soil, and air [22]. Therefore, the use of chitosan as an instrument for the ecologic control of phytopathogenic microorganisms is an interesting alternative [22,26]. At present, there are very few studies of chitosan ultrasound-assisted extraction (UAE) from *Litopenaeus vannamei* chitin, and even fewer tested on *P. ultimum* growth inhibition. Hence, this study focusses on obtaining chitosan by the UAE methodology from white shrimp (*Litopenaeus vannamei*) chitin, as well as the physicochemical and structural characterization of the obtained chitosan, and its effect on the inhibition of *P. ultimum* radial growth.

2. Materials and Methods

2.1. Biologic Material

White shrimp (*Litopenneaus vannamei*) exoskeletons were collected from aquaculture farms in Yucatán (21°12′01.1″ N, 89°57′00.6″ W) and transported to the Food Safety and Traceability Laboratory at the Southeast Unit of the Center for Research and Assistance in Technology and Design of the State of Jalisco, AC (Mérida, México). The collected material was thoroughly washed with fresh tap water to remove most of the impurities acquired during handling. Subsequently, the material was

dehydrated in an electric convection oven (Jersa—No. 148-09, Mexico, Mexico) for 12 h at 50 °C and ground using a blender (Osterizer Galaxie 4107/869-16G, Mexico, Mexico); the resulting powder was sieved through a 0.0197 in (0.05 cm) mesh and stored in plastic bottles until its proximal analyses (moisture, ash, and protein). The *Pythium ultimum* strain (P233.08) was obtained from The Czech Collection of Phytopathogenic oomycetes bank of The Silva Tarouca Research Institute for Landscape and Ornamental Gardening (RILOG). The strain was grown for 14 days in potato dextrose agar (PDA). The sodium hydroxide (NaOH) and boric acid (H_3BO_3) were obtained from the Golden Bell company (Jalisco, Mexico), hydrochloric (HCl) and sulfuric acid (H_2SO_4) from J.T. Baker (Xalostoc, Mexico state, Mexico). High molecular weight chitosan (CC) and PDA media were purchased from Sigma-Aldrich (St. Louis, MO, USA).

2.2. Chitin Extraction

Chitin extraction was performed following the procedure reported by Robles et al. [27]. Briefly, shrimp exoskeleton demineralization was carried out with 2 M HCl solution at a ratio of 1:20 (w/v) under magnetic stirring for 3 h at 25 °C. Subsequently, the solids were filtered using a Buchner funnel and Whatman No. 4 filter paper. The exoskeletons were treated with a 2 M NaOH solution at a ratio of 1:10 (w/v), and the mixture kept under magnetic stirring for 24 h at 25 °C for deproteinization. The mixture was neutralized with 2 M HCl, and then precipitated chitin was separated from the liquid by decantation. The chitin was vacuum filtered and dried in an oven (OV-12, Jeio Tech Co., Ltd., Geumcheon-gu, Seoul, Republic of Korea) for 12 h at 50 °C. Finally, the chitin was screened through a 0.0197 in mesh, and stored in plastic bottles at 25 °C. The extraction yield was calculated according to Equation (1) and expressed as a percentage.

$$Yield\ (\%) = \frac{Recovered\ chitin\ (g)}{100g\ Exoskeletons} \times 100 \tag{1}$$

2.3. Factorial Design for the UC Obtention

A 2^3 factorial design was performed to determine the best deacetylation conditions. The factors evaluated were: NaOH concentration (50% and 65%), wave amplitude (75% and 90%), and sonication intervals (5 min and 7.5 min). The intervals were applied as follows: (1) 5 min of sonication per 5 min of repose, and (2) 7.5 min of sonication per 5 min of repose, both for the 90 minutes of total reaction [9]. The response variables measured were: extraction yield, and solubility of the resulting product in aqueous acetic acid solution (1% v/v), considering as chitosan material with a solubility higher than 65%. The reaction was carried out in a 50 mL Eppendorf™ conical tube using one gram of chitin and 45 mL of NaOH solution, and transferred to the ultrasound equipment (model GEX130PB, 130 W–20 kHz, Newtown, CT, USA) coupled to a 13 mm diameter probe. The sonication and magnetic intervals remained until reaching 90 min of reaction [9]. Two different chitosan as control treatments were obtained by the conventional chemical method (magnetic stirring for 5 h at 90–100 °C) [20]. Then all mixtures were cooled in an ice bath for 30 min and neutralized with HCl solution (50% v/v). The solids were recovered by filtration and kept in plastic bottles at 25 °C until further characterization.

2.4. Physicochemical Characterization

2.4.1. Chitosan Solubility

Chitosan solubility was determined as reported by Singh et al. [13]. A solution was prepared with 0.1 g of chitosan in 40 mL of aqueous acetic acid at 1% (v/v). The mixture was kept in constant agitation for 18 h, and then vacuum filtered through a Whatman No. 4 filter paper (previously dried at 100 °C for 12 h and weighed); the insoluble material retained in the filter paper was dried and weighed to obtain the solubility percentage, according to Equation (2):

$$Solubility\ (\%) = \frac{(P_1 + M) - P_2}{M} \times 100 \tag{2}$$

where P_1 is the dry weight of the filter paper (g), P_2 is the dry weight of the filter paper, and the retained insoluble material (g), and M is the initial weight of the chitosan (g).

The yield of chitosan was calculated by Equation (3).

$$Yield~(\%) = \frac{Recovered~chitosan~(g)}{100g~Chitin} \times 100 \tag{3}$$

2.4.2. Total Nitrogen Determination and Protein Content

The total nitrogen content was estimated by the Kjeldahl method [11] using an automated digestor DKL 12 series and UDK 129 distillation unit (Scientifica Srl. Usmate (MB), Usmate Velate (MB), Italy). Digestion was carried out with 2 g of the sample in 12 mL of concentrated sulfuric acid, 5 mL of hydrogen peroxide (30% v/v), and one catalyst tablet at 420 °C for 60 min. The nitrogen in the sample was converted into ammonium (NH_4^+), then released as ammonia (NH_3) during distillation, and finally collected in a boric acid solution (4% w/v). After titration with a 0.2 N HCl solution, the total nitrogen content was calculated by Equation (4). For protein content, the value was obtained as the difference in the nitrogen content of the samples and the nitrogen content in commercial chitin (CC), and multiplied by the factor 6.25 provided by the method, resulting in the total or residual protein content in the samples.

$$Nitrogen~(\%) = \frac{V \times N \times 0.014 \times 100}{M} \tag{4}$$

where here V is the volume of the HCl consumed in the titration (mL), N is the HCl normality, M is the weight of the sample (g), and 0.014 refers to the nitrogen milliequivalents.

2.4.3. Ash Content Determination

The ash content was determined according to the Association of Official Agricultural Chemists (AOAC) official method 942.05 [28]. The ground materials were dehydrated at 90 °C for 5 h until constant weight. Subsequently, the samples (3 g) were placed in porcelain crucibles and burned in a muffle (Felisa FE-363, Mexico, Mexico) at 500 °C for 2 h. The ash content was calculated according to Equation (5).

$$Ash~(\%) = \frac{(P - p) \times 100}{M} \tag{5}$$

where P is the weight of the crucible with the calcinated sample (g), p is the weight of the empty crucible (g), and M is the mass of the sample (g).

2.5. Structural Characterization

2.5.1. Degree of Deacetylation (DDA)

The DDA determination was carried out by ^{1}H NMR spectroscopy [29] and Fourier transform infrared spectroscopy (FTIR) analysis [7,30]. For the ^{1}H NMR analysis, the ratio between the intensity (I) of the methyl-(1-4) 2 acetamido-2-deoxy-β-D-glucan proton signals and the reference of protons H-2 to H-6, was calculated using Equation (6). The ^{1}H NMR spectra were obtained at 80 °C using a Bruker AVANCE III spectrometer (υ = 400 MHz) (Bruker, Avance III, Wissembourg, France). The sample was prepared by dissolving 10 mg of chitosan in 1% (v/v)/D2O HCl solution, which was kept under constant agitation overnight. Next, an aliquot was taken for analysis [11].

$$DDA = \frac{\frac{1}{3} I_{CH_3}}{\frac{1}{6} H_2 - H_6} \times 100 \tag{6}$$

For the FTIR analysis, a spectrometer (Agilent Cary 630) in attenuated total reflectance mode, in the 600 cm^{-1} to 4000 cm^{-1} wavelength range, was used. The DDA was determined using the correlation between the intensity of the band at 1655 cm^{-1} (amide I), and the band at 3450 cm^{-1} (O–H),

according to Equation (7) (Baxter equation) [2,7,30]. Additionally, DDA was also calculated using Equation (8), which refers to the degree of acetylation (DA). Equation (9) was used to estimate the DDA [7].

$$DDA = 100 - \left(\frac{A_{1655}}{A_{4350}} \times 115 \right) \tag{7}$$

$$\frac{A_{1320}}{A_{1420}} = 0.3822 + 0.03133\,DA \tag{8}$$

$$DDA = 100 - DA \tag{9}$$

2.5.2. Molecular Weight (M_W) Determination

The M_W determination was performed by size exclusion chromatography (SEC) using gel permeation equipment (Waters 410) equipped with an IsoChrom LC pump, connected to gel packed columns (TSK2500 y TSK6000, Tosoh Bioscience), and a refractive index refractometer operating at 632.8 nm. The chitosan was dissolved (0.5 g L^{-1}) in a buffer solution of ammonium acetate (0.15 mol L^{-1}) and acetic acid (0.20 mol L^{-1}), pH = 4.5, which was also employed as eluent at a flow rate of 0.5 mL min^{-1}. These solutions were filtered through a 0.45 μm cellulose acetate membrane (Millipore™), and injected into the columns (v = 100 μL) [11]. The M_W value was determined with the increase of the refractive index dn/dc for chitosan in the range of 0.19 cm^3 g^{-1} to 0.183 cm^3 g^{-1}, according to the DA of the chitosan [5].

2.5.3. X-ray Diffraction Analysis (XRD)

The XRD patterns of the samples were determined using a Bruker Diffractometer (Bruker AXS, model D8 Advance, Karisruhe, Germany) (CuKa, λ = 1.5418 Å, range 2θ = I–50°, at a speed of 1°/min, 40-keV, and 40 mA) [11,13]. The crystallinity index (*Icr*) was calculated using Equation (10):

$$I_{cr} = \left[\frac{I_{110} - I_{am}}{I_{110}} \right] \times 100 \tag{10}$$

where I_{am} is the diffraction intensity in the amorphous area at 16°, and I_{110} is the maximum intensity in the crystalline region at 20° [11,13].

2.6. Inhibitory Effect of the Chitosan

The effect of chitosan on the inhibition of the radial growth of *P. ultimum* was evaluated following a methodology proposed by Pacheco et al. [5], with slight modifications. The test was carried out in 10 cm diameter Petri dishes, with PDA culture medium (39 g L^{-1}) supplemented with 2.5 g L^{-1} of chitosan obtained by UAE (UC). The positive control was evaluated by supplementing the PDA medium with 2.5 g L^{-1} of commercial chitosan (CC), and the negative control consisted of PDA culture medium without the addition of chitosan, tests were performed by triplicate. The culture mediums were sterilized in an automatic vertical autoclave (Ecoshel, CVQ-B35L, Mexico, Mexico) at 121 °C and 15 lb(in^2)$^{-1}$ for 15 min, then samples were placed into sterile Petri dishes in a horizontal laminar flow hood (LABCONCO, Kansas, USA). Culture mediums were inoculated with PDA cubes (~5 × 5 cm) containing *P. ultimum* mycelia at the exponential growth stage, and incubated for 120 h at 30 °C. The measurements of mycelial growth were performed every 24 h, and the results were expressed as radial growth (cm) and the percentage of radial inhibition (RI %), according to Equation (11). Radial growth values were also fitted to the Gompertz model (Equation (12)) to obtain kinetic parameters of the radial growth, such as growth rate (k_R) and maximum radial growth (RG$_{MAX}$), using the origin Pro program (version 2019; OriginLab Corporation, Northampton, Ma, USA) [5].

$$\% \; Inhibition = \left(1 - \frac{Radial\;growth\;of\;the\;treatment_T}{Radial\;growth\;of\;the\;control_T} \right) \times 100 \tag{11}$$

where *T* is the time evaluated.

$$y(t) = a\exp(-\exp(-k(t-tc)))\qquad(12)$$

where y(t) is the radial growth of *P. ultimum* (cm) at time (t); "a" is the RG_{MAX}; tc is a constant related to the initial conditions when t = 0 (initial time), and k corresponds to k_R (h^{-1}).

2.7. Statistical Analysis

The studies were conducted by triplicate using a randomized experimental design 2^3. The results obtained were subjected to analysis of variance (ANOVA), and to the comparison of means by Least significant Difference Test (LSD), with a significance of $p \le 0.05$, using Statgraphics Centurion XVI software (Statistical Graphics Corp., Manugistics, Inc., Cambridge, MA, USA).

3. Results

3.1. Chitosan Obtained by UAE

The solubility and yield extraction of the deacetylated samples obtained by UAE of chitin, and the two treatments obtained by the conventional deacetylation process are shown in Table 1. The treatments displayed variation in the solubility values, ranging from 7.37% to 100% (being the highest value), similar to that obtained for the CC. The chitosan obtained by the conventional chemical method presented a solubility of 58.72% for NaOH concentration of 50% (w/v), and 85.40% for NaOH 60% (w/v). The evaluated variables had a significant effect on the solubility of the products obtained ($p \le 0.05$). The highest solubility was achieved when using NaOH at 65% (w/v), regardless of the amplitude and sonication interval (Table 1). Treatments 7 and 8 presented the highest values in both response variables. The Pareto analysis (Figure 1) showed that the solubility of the chitosan increased by increasing the NaOH concentration, similarly to the conventional method. The same effect was observed with the increment of the amplitude.

The sonication time presented an effect on the reaction temperature (Figure 1). The UC T7 displayed the highest yield (86.89%) and degree of solubility (100%) in a shorter time (sonication interval 5–5) compared to the different treatments, with a longer time (7.5–5). The deacetylation conditions employed for the preparation were used to evaluate temperature dependence. The temperature behavior indicated an accelerated increase during the first 30 min, reaching a steady-state at that time, and remaining constant until 90 min.
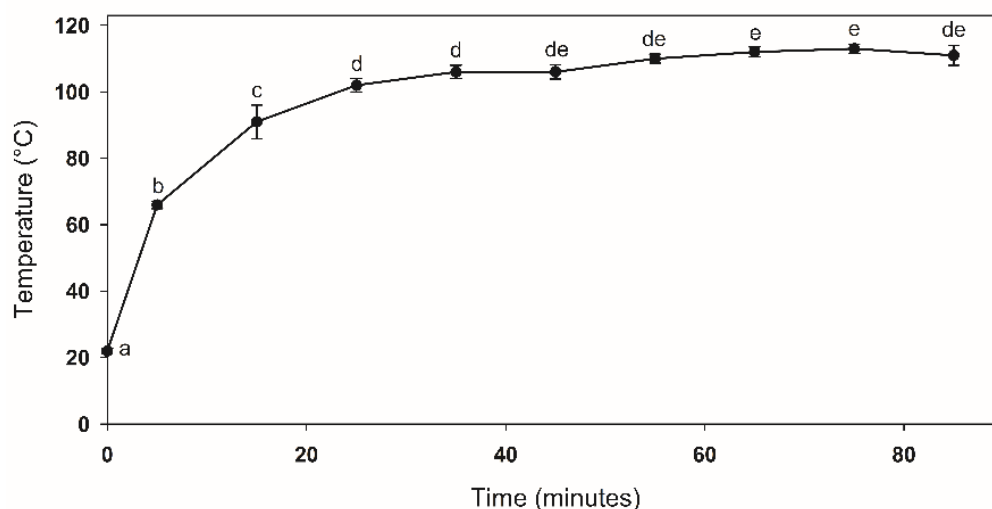
Figure 1. (•) Reaction temperature during ultrasonic irradiation according to the conditions: NaOH 65% (w/v), 90% amplitude, and sonication interval of 5–5 min (UC T7).

Table 1. Solubility and extraction yield results from the different biopolymers obtained (partial deacetylated chitin and chitosan) by ultrasound-assisted extraction (UAE) and conventional methods.

Treatment (Code)	Factor			Response	
	Amplitude (%)	NaOH (%)	Interval (min) A [1]–B [2]	Solubility (%) [3]	Yield (%)
UC T1	75	50	5–5	13.42 ± 3.5 [a]	<15 ± 3.91 [a]
UC T2	75	50	7.5–5	7.37 ± 2.6 [a]	<15 ± 5.29 [a]
UC T3	90	50	5–5	42.8 ± 1.7 [c]	20.65 ± 0.82 [a]
UC T4	90	50	7.5–5	20.79 ± 0.6 [b]	17.26 ± 0.5 [a]
UC T5	75	65	5–5	98.0 ± 0.1 [f]	80.32 ± 0.08 [b]
UC T6	75	65	7.5–5	97.9 ± 0.3 [f]	81.05 ± 0.25 [b]
UC T7	90	65	5–5	100 ± 0.0 [f]	86.89 ± 0.0 [c]
UC T8	90	65	7.5–5	94.8 ± 4.2 [f]	87.21 ± 3.86 [c]
CC	ND	ND	ND	100 ± 0.0 [f]	ND
Conventional Chitosan	ND	50	300	58.72 ± 0.9 [d]	88.35 ± 1.35 [c]
Conventional Chitosan	ND	60	300	85.40 ± 0.7 [e]	87.5 ± 0.72 [c]

[1] Sonication period; [2] Repose period; [3] Values are the average result of three measurements; Superscript letters indicate no significant differences between results by the LSD analysis; UC: ultrasound chitin or chitosan (solubility values lower than 50% are considered as partially deacetylated chitin biopolymer, while higher solubility values than 50% refer to a chitosan biopolymer); ND: Non determined. The solubility and yield percentages were calculated using Equations (2) and (3), respectively.

3.2. Physicochemical and Structural Characterization

Following the previous results, the physicochemical characterization was performed on chitosan obtained with the conditions of UC T7, as it exhibited a 100% solubility and high extraction yield in the short period evaluated, which could lead to a minor energy consumption. The total nitrogen in the molecule was 8.7%, corresponding to the total nitrogen presented in the chitosan molecule, indicating complete protein removal. The ash content obtained was less than 5%.

3.2.1. Determination of the DDA

The ^{1}H NMR spectrum of the UC of T7 (Figure 2) showed one peak at 2.0 ppm related to the methyl protons from the acetylated glucosamine residue; peaks between 3.6 ppm and 4.1 ppm correspond to the C-3, C-4, C-5, and C-6 protons from the pyranose ring. Peaks at 3.1 ppm and 4.8 ppm were related to protons C-2 and C-5 from the glucosamine residue [14]. The resulted DDA, obtained by the ^{1}H NMR spectrum for the UC treatment (85.25%), was higher than that obtained for the CC (83%). On the other hand, the FTIR spectra for UC and CC showed the characteristic absorption bands around 3328 cm^{-1} and 3256 cm^{-1}, corresponding to the C–O and N–H stretching [31], and the C–O group at 3439 cm^{-1} and 3425 cm^{-1}, respectively [32,33] (Figure 2). The band at 2924 cm^{-1} corresponded to the CH_2 and CH_3 groups [31], attributed to C–H asymmetric and symmetric stretching [7,13,34]. The bands at 1700 cm^{-1} (UC) and 1634 cm^{-1} (CC) were most likely to represent the amide-I band (C-O in the NH-$COCH_3$ group) previously reported at 1640 cm^{-1}, 1657 cm^{-1}, and 1647 cm^{-1} to 1654 cm^{-1} [31,35]. The bands located at 1570 cm^{-1} (UC) and 1560 cm^{-1} (CC) were attributed to the N–H bending vibrations of the NH-$COCH_3$ group (Amide II band). The weakened peak indicated successful deacetylation of the chitin [31,35]. The band of saccharide around 1148 cm^{-1} was due to the antisymmetric stretching of the C–O–C bridge. C–O stretching of the structure was observed at 1010 cm^{-1} and 1065 cm^{-1} [7]. The band located at 890 cm^{-1} was due to the C–H β-glycosidic bond out of plane vibration [35].
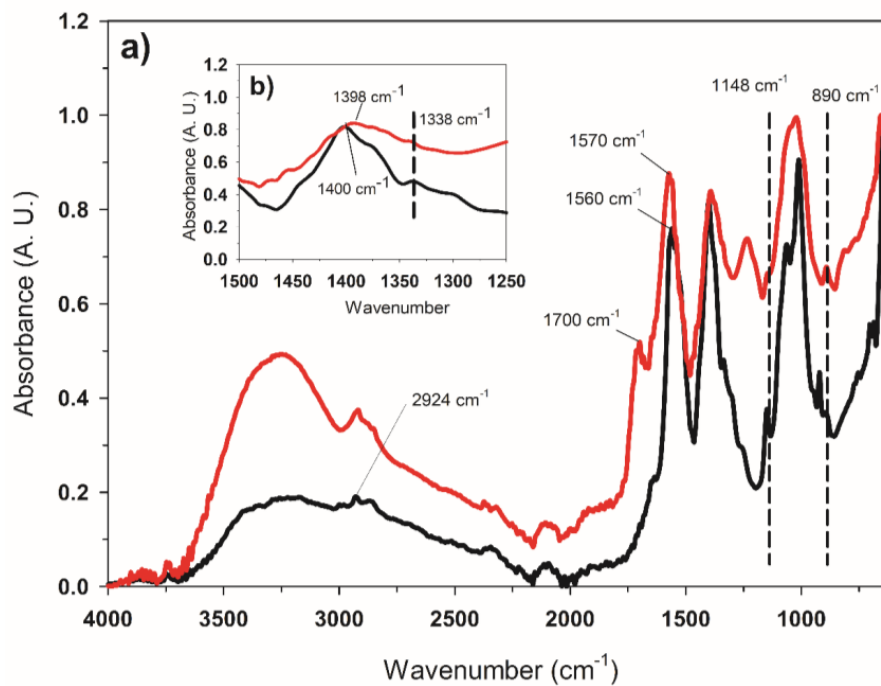
Figure 2. FTIR spectra of (**a**) CC (–) and UC (–) in the range between 4000 cm^{-1} and 500 cm^{-1}, (**b**) of CC (–) and UC (–) in the range between 1500 cm^{-1} and 1250 cm^{-1}.

3.2.2. Determination of the M_W and X-ray Diffraction Analysis

The M_W obtained by size-exclusion chromatography (SEC) for the UC was 3.928×10^5 (g/mol), corresponding to a high M_W biopolymer [5]. The results suggest that the UAE diminished the depolymerization and allowed the obtention of chitosan with a high M_W. The XRD patterns of CC and UC are shown in Figure 3. Both samples exhibit two crystalline planes at $2\theta \approx 9.8°$ and $2\theta \approx 19.7°$, a shoulder also appears in the spectrum at $2\theta \approx 21.7°$. Crystallinity indexes were calculated from the X-ray diffraction data, and they were 83% and 87%, for CC and UC, respectively.
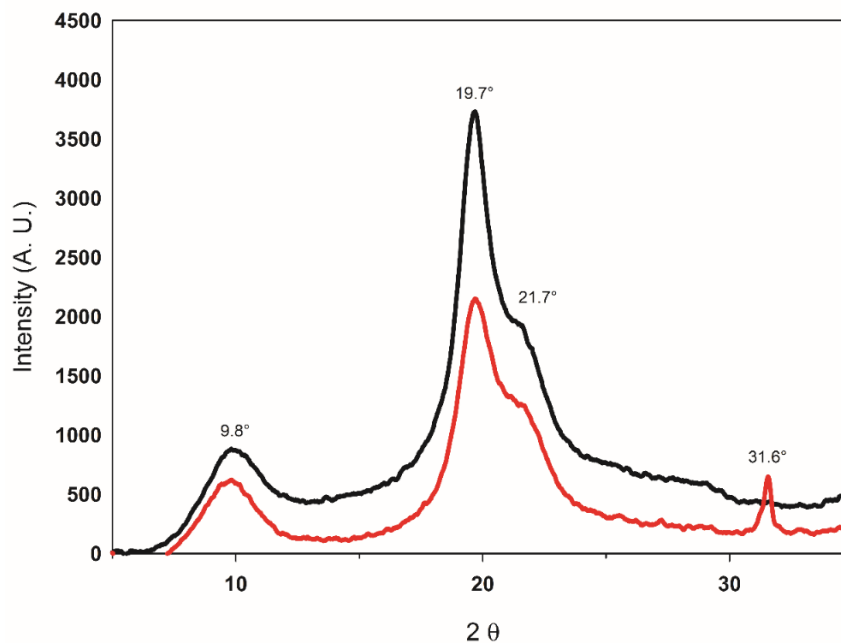
Figure 3. X-ray diffractograms of the CC (–) and UC (–).

3.3. Inhibitory Activity of the Chitosan

After 72 h, the full growth of *P. ultimum* in the negative control (only PDA) was observed. While for the treatment PDA + UC and PDA + CC, the percentages of inhibition were 85.98% and 100%, respectively (Table 2). According to the results, the lag phase of *P. ultimum* growth was extended until 48 h on treatment with PDA + UC, while PDA + CC was able to inhibit the growth for 96 h. Therefore, PDA + CC presented a higher static effect on the growth of *P. ultimum* in comparison to PDA + UC. However, at 96 h both samples exhibited a similar inhibition percentage on the radial growth (80% and 77.65%, respectively). Figure 4 shows the radial growth of *P. ultimum* during the time course, the k_R, RG_{MAX}, and R^2, obtained by the fitting of the Gompertz model displayed by Pacheco et al. [11], with modifications. Although the RG_{MAX} obtained for the CC was lower than the UC sample, the k_R value for the UC sample was lower than the CC, indicating that even though both samples produced a reduction in the maximal radial growth, the presence of the UC had a major effect on the growth rate of the microorganism, rather than in the lag phase, as it was possible to observe in the CC chitosan.

Table 2. *Pythium ultimum* inhibition according to the time course.

Time (h)	PDA + UC	PDA + CC
24	98.92% [a]	100.00% [a]
48	93.00% [b]	100.00% [a]
72	85.98% [b]	100.00% [a]
96	77.65% [a]	80.00% [a]
120	64.62% [b]	72.06% [a]

Different letters in the same column indicate a significative difference ($p \leq 0.05$) by LSD Test; PDA: Potato Dextrose Agar; UC: ultrasound chitosan; CC: Commertial chitosan.

Treatment	k_R (h^{-1})	RG_{MAX}	R^2
Control	0.141	3.68	0.99
PDA+CC	0.093	1.22	0.99
PDA+UC	0.018	2.77	0.99
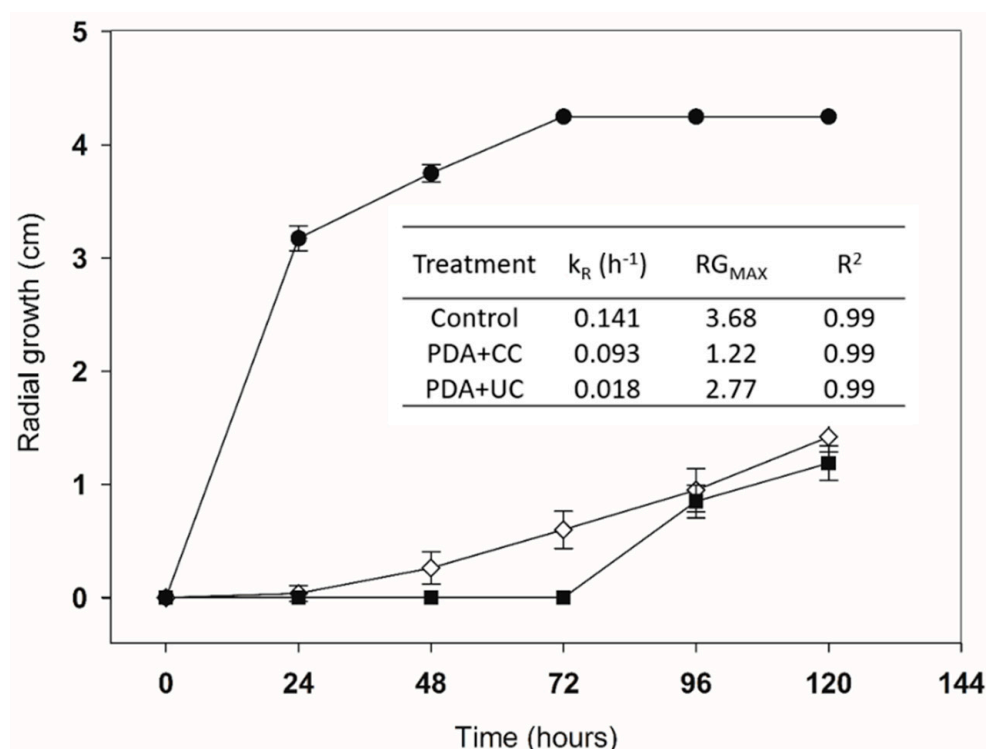
Figure 4. (●) Radial growth of *P. ultimum* in control medium (PDA); *P. ultimum* radial growth in PDA medium using (◊) 2.5 g/L UC and (■) 2.5 g/L CC, and presentation of kinetics parameters of radial growth estimated by the Gompertz model.

4. Discussion

Chitosan yields obtained by sonication were similar to those obtained employing the conventional chemical method. The UAE proved to be an efficient method for the chitin deacetylation, requiring less reaction time compared to the conventional process, and reducing energy consumption, as reported by Birolli et al. [9] and Ngo and Ngo [8]. The above was associated with the increment of the accessibility to the reactive sites through the phenomenon of cavitation by the irradiation. This phenomenon also induces the chitin particles fragmentation and swelling, increasing the particle surface area [10,36]. Additionally, this process favors the reduction of molecular oxygen concentration during the sonication process, and therefore, the occurrence of undesirable reactions, like oxidative depolymerization [37].

Regarding chitosan characterization, the nitrogen content of the UC presented a similar value as has been reported for chitosan from shell crab [38] and shrimp [1], both materials obtained through conventional chemical extraction. In the FTIR spectrum, the absence of the band around 1540 cm^{-1} indicates an effective protein removal during the deproteinization process. This band is characteristic of the N-acetyl groups and corresponds to the N–H bending of amide-II, and it was not observed in the UC spectrum [39]. On the other hand, the ash content exhibited by the UC (<5%) had a similar value to that reported by Abdel-Rahman et al. [40] for chitosan from shrimp exoskeletons. However, chitosan extracted from shrimp shells by the chemical-biologic method presented an ash content of 1.9% [11], and the values reported by Huang et al. [32] ranged from 0.052% to 0.176%. The variation in the ash content depends mainly on the source and material composition. Kumari et al. [1] suggested that low ash content in chitosan tends to improve its solubility; meanwhile, high ash contents tend to reduce the viscosity and molecular weight.

The DDA of chitin and chitosan biopolymers is an important parameter that defines their applications and name. The term chitosan should be used when the biopolymer exhibits a DDA greater than 70% [41,42]. The DDA values of the UC obtained by ^{1}H NMR spectroscopy were higher (85.25%) than those obtained for the CC (83%). In the UC ^{1}H NMR spectrum (Figure 3) the disappearance of a peak around 4.9 ppm (H1-A), which represents the H1 proton of the acetylated monomer, is indicative of high deacetylation [13,43]. This can be attributed to the influence of the amplitude, irradiation time, and temperature achieved during the deacetylation process (<105 °C) [6,37]. The FTIR spectrum (Figure 4) shows the absorption peaks 1320 cm^{-1} and 1420 cm^{-1} that are also used to calculate chitosan DDA (A_{1320}/A_{1420}), with a minor error, with more sensitivity to the chemical composition and regardless of technique, state, and secondary structure, as reported by Brugnerotto et al. [44]. The characteristic band at 1319 cm^{-1} to 1323cm^{-1} of the FTIR spectrum corresponds to the amide-III band [32,35]. However, for the UC and CC, the characteristic band at 1338 cm^{-1} (amide III) was used as a reference band of the methyl groups from 1390 cm^{-1} to 1400 cm^{-1}, which were reported in previous works [44]. The calculated values for the DDA using the Brugnerotto Equation (7) were 88% and 86%, for UC and CC, respectively, while the Baxter Equation (6) showed values of 78% and 67%, for the UC and CC, respectively. The difference between the values obtained by the equations may be attributed to the chitosan moisture concentration [7]. Similar results to those obtained by UAE were observed with different sources of chitin [9]. The DDA values obtained by the two techniques (^{1}H NMR and FTIR) presented similar behavior.

As the M_W of chitosan affects its physicochemical and functional properties, as well as its applications [38], this is an important parameter to be considered for its characterization. The variation in M_W values may be caused by the DDA, the source, the temperature, type, time and alkali concentration of the deacetylation process, previous treatments, and particle size, among others [45]. The M_W value obtained for UC (3.928×10^5 g mol^{-1}) locates within the range reported (1×10^5 g mol^{-1} to 5×10^5 g mol^{-1}) in different studies [13,46]. While chitosan obtained from shrimp exoskeletons through the conventional extraction method exhibited a M_W value of 2.20×10^5 g mol^{-1} [45].

The molecular structure and functionality of chitosan can be further investigated by XRD, as it is an outstanding crystalline biopolymer among all other carbohydrate polymers, with a strong intermolecular hydrogen-bonds [47]. The diffractograms obtained for UC and CC showed crystalline

planes at 2θ ≈ 9.8° and 2θ ≈ 19.7°, indicating the structure of a semi-crystalline biopolymer [1,36,38]. The shoulder observed at 2θ ≈ 21.7° may be due to the origin of chitin [38,48]. In the literature, some chitosan DRX patterns presented two characteristic peaks, usually around at 2θ ≈ 10° and 20° [45]. In other reports, these peaks were observed at 2θ ≈ 20.2° and 2θ ≈ 22.4°, such as for shrimp (*Metapenaeus stebbingi*) exoskeletons [45]. The appearance of this shoulder has also been observed as the DDA increases with the addition of more UAE steps, evidencing a hydrated crystalline allomorphic chitosan [36]. Regarding the *Icr* (87%), the value obtained for UC was higher compared to the reports in the literature [7,13], indicating that the extraction process was suitable to maintaining the crystalline structure of the biopolymer. An *Icr* value as low as 27% has been reported when reaching high temperatures during UAE, due to heating under alkaline conditions, which can distort chitin structure and chain arrangements [13]. Other methods to obtain chitosan, such as microwave irradiation, have shown *Icr* values of up to 56% [7]. While the use of the conventional extraction methods may produce chitosan with an *Icr* value of 75% from shrimp chitin [49]. The difference of the *Icr* values obtained and the ones found in the literature is attributed to inter-molecular bonds present after deacetylation. Moreover, the molecular structure could have been in a predominantly crystalline arrangement, unlike other reports that present an amorphous predominance [50]. One of the most important effects of the crystallinity lies in the biological activities of the chitosan, such as the antimicrobial effect; as depending on the source of the material, the different molecular arrangements in the structure of the biopolymer may cause electrostatic interaction with the microbial cell walls [19].

Regarding the inhibitory effect on *P. ultimum*, it was observed that CC maintained the oomycete in the lag stage for a more extended period than the UC. The above was attributed to the availability of the acetyl groups, attributed to a lower *Icr* and M_W of CC than UC [51,52]. This effect is related to a higher number of protonated groups available to interact with the microbial cells [42,53]. Three mechanisms have been proposed to explain the inhibitory activity of chitosan; (1) the functional groups in the chitosan interact with the phospholipids in the fungi membrane, causing leakage of cellular content; (2) chitosan activates essential chelating elements that cause the lack of nutrients, and finally, (3) by penetrating the cell wall and interacting with the DNA, affecting the synthesis of proteins [54]. It has been reported that deacetylation carried out under heterogeneous conditions causes an irregular distribution of glucosamine residues in the chitosan, resulting in a degree of aggregation and solubility that affects the biological properties, resulting in differences in samples with the same DDA [54]. The above could explain why both chitosan (with similar DDA and M_W) maintained *P. ultimum* in the lag stage at different times. Nevertheless, the exponential growth of the oomycete was faster for CC than UC. The above may be attributed to the fact that after a certain time chitosan also acted as a nutrient after its complete interaction with *P. ultimum*, as reported by Palma-Guerrero et al. [55]. In contrast, a higher crystallinity of UC than CC affects the inhibitory activity of chitosan, since the different molecular rearrangements in a biopolymer may affect electrostatic interaction between the cell walls of microorganisms [19]. Similar behaviors have been reported elsewhere [5,56]; on the inhibition of phytopathogen microorganisms at 2500 μg mL^{-1} and 2180 μg mL^{-1}, respectively. According to previous studies, chitosan is a biopolymer that exhibits inhibitory activity on several phytopathogenic microorganisms (i.e. fungi and oomycetes) [57]. In this sense Xu et al. [57] reported the chitosan inhibitory activity in in-vitro tests on mycelial growth of the phytopathogenic microorganisms, *Botrytis cinerea* and *Phytophthora capsici*, using Petri dishes with PDA culture medium. Inhibitory activity (EC50) on *Phytophthora capsici* and *B. cinerea* were observed at a chitosan concentration of 580 μg/mL and 1640 μg mL^{-1}, respectively. The Oligochitosan employed (300,000–500,000 Da, DDA > 95%) increased the inhibitory activity as the concentration of the biopolymer augmented from 100 μg mL^{-1} to 580 μg mL^{-1}. Similarly, Park et al. [58] evaluated the inhibition of the radial growth of *P. irregulare*, using chitosan with different DDA (57.3% to 99.2%) in a range from 100 μg mL^{-1} to 1000 μg mL^{-1}. Meanwhile, Pacheco et al. [5] evaluated the inhibition of *Penicillium digitatum* at a chitosan concentration of 2500 μg mL^{-1} (107,000 Da; DDA = 66.2%), this suggests an increased activity with a lower value of M_W and a higher value of DDA. The polycationic nature of chitosan can act on the cell wall, altering

the osmotic pressure of several phytopathogens. This behavior was reported by Xu et al. [57] as a possible mechanism of the inhibitory activity of the chitosan on *P. capsica*, as it provoked damage to hyphae tips, essential structures for the growth of oomycetes. Badawy and Rabea [56] reported the inhibitory activity of chitosan (DDA > 89%) on *P. debaryanum* at a concentration of 2180 μg mL^{-1}. The in vitro tests evaluated by Pacheco et al. [5] showed the biological potential of chitosan (107,000 Da) when combined with *Pichia guillermondii* to inhibit *P. digitatum*. Furthermore, the use of chitosan as a biocontrol agent offers different mechanisms of protection, such as growth stimulation, improvement of the photosynthetic activity, and accumulation of secondary metabolites, which provides additional protection against biotic and abiotic stress in plants [59]. Finally, the use of this material in conjugation with other compounds, such as chitosan-based nanoparticles or biopolymer agents, is an option for the development of precision agriculture, and the reduction of pesticide usage [60].

5. Conclusions

UAE is an alternative and viable option for the obtention of chitosan with high yields. Furthermore, the biopolymer obtained (UC) was characterized by being 100% soluble, presenting a high M_W in comparison to CC. The DDA values calculated by different methods were higher than 78%, and the XRD analysis allowed us to calculate an *Icr* value of 87%. It was also observed that the effect of the temperature during UAE resulted in a higher degree of solubility and yield of extraction. On the other hand, although the inhibitory effect of the UC on the growth of *P. ultimum* was minor, compared to CC during the first 72 h, the *Icr* value of the chitosan allowed keeping the inhibition constant, and comparable to CC. Hence, there may be a significant factor in the mechanism of the inhibitory activity. The UC exhibited promising results; however, further studies are needed to fully comprehend the action mechanism of the chitosan against *P. ultimum,* and the enhancement that could occur by the conjugation of UC with other compounds to inhibit the growth of the oomycete.

Author Contributions: Conceptualization, N.P., N.M.-T. and H.M.-L.; methodology, H.M.-L., E.H.-P., S.T., N.M.-T., A.R.-D., J.C.C.-B. and N.P.; formal analysis S.C.P.-C., H.M.-L., E.H.-P., N.M.-T. and N.P.; investigation, T.A.-T., J.C.C.-B. and N.P.; resources, T.A.-T., H.E.-A., S.T. and N.P.; data curation, H.M.-L., E.H.-P., S.C.P.-C., S.T., N.M.-T.; writing—original draft preparation, H.M.-L., S.C.P.-C. and E.H-P.; writing—review and editing, S.C.P.-C., J.C.C.-B., A.R.-D, T.A.-T., H.E.-A. and N.P.; visualization, N.P., N.M.-T. and H.M.-L.; supervision, T.A.-T., H.E.-A., A.R.-D., S.T. and N.P.; project administration, T.A.-T., H.E.-A. and N.P.; funding acquisition, T.A.-T., H.E.-A., S.T. and N.P. All authors have read and agreed to the published version of the manuscript.

References

1. Kumari, S.; Kumar Annamareddy, S.H.; Abanti, S.; Kumar Rath, P. Physicochemical properties and characterization of chitosan synthesized from fish scales, crab and shrimp shells. *Int. J. Biol. Macromol.* **2017**, *104*, 1697–1705. [CrossRef]

2. Said Al Hoqani, H.A.; AL-Shaqsi, N.; Hossain, M.A.; Al Sibani, M.A. Isolation and optimization of the method for industrial production of chitin and chitosan from Omani shrimp shell. *Carbohydr. Res.* **2020**, *492*, 108001. [CrossRef]

3. Rinaudo, M. Chitin and chitosan: Properties and applications. *Prog. Polym. Sci.* **2006**, *31*, 603–632. [CrossRef]

4. Domard, A. A perspective on 30 years research on chitin and chitosan. *Carbohydr. Polym.* **2011**, *84*, 696–703. [CrossRef]

5.   Pacheco, N.; Larralde-Corona, C.P.; Sepulveda, J.; Trombotto, S.; Domard, A.; Shirai, K. Evaluation of chitosans and *Pichia guillermondii* as growth inhibitors of *Penicillium digitatum*. *Int. J. Biol. Macromol.* **2008**, *43*, 20–26. [CrossRef] [PubMed]

6.   Tahtat, D.; Boutrig, H.H.; Khodja, A.N.; Benamer, S.; Hammache, Y.; Mahlous, M. The synergistic effect of gamma irradiation and alkaline soaking at low temperature on the pre-deacetylation of α-chitin: Optimization by design of experiment. *Carbohydr. Polym.* **2019**, *215*, 39–46. [CrossRef]

7.   El Knidri, H.; El Khalfaouy, R.; Laajeb, A.; Addaou, A.; Lahsini, A. Eco-friendly extraction and characterization of chitin and chitosan from the shrimp shell waste via microwave irradiation. *Process Saf. Environ. Prot.* **2016**, *104*, 395–405. [CrossRef]

8.   Ngo, T.H.D.; Ngo, D.N. Effects of low–frequency ultrasound on heterogenous deacetylation of chitin. *Int. J. Biol. Macromol.* **2017**, *104*, 1604–1610. [CrossRef]

9.   Birolli, W.G.; Delezuk, J.A.D.M.; Campana-Filho, S.P. Ultrasound-assisted conversion of alpha-chitin into chitosan. *Appl. Acoust.* **2016**, *103*, 239–242.

10. Hafsa, J.; Smach, M.A.; Charfeddine, B.; Limem, K.; Majdoub, H.; Rouatbi, S. Antioxidant and antimicrobial proprieties of chitin and chitosan extracted from Parapenaeus Longirostris shrimp shell waste. *Ann. Pharm. Françaises* **2016**, *74*, 27–33. [CrossRef]

11. Pacheco, N.; Garnica-Gonzalez, M.; Gimeno, M.; Bárzana, E.; Trombotto, S.; David, L.; Shirai, K. Structural characterization of chitin and chitosan obtained by biological and chemical methods. *Biomacromolecules* **2011**, *12*, 3285–3290. [CrossRef] [PubMed]

12. Harris, R.; Lecumberri, E.; Mateos-Aparicio, I.; Mengíbar, M.; Heras, A. Chitosan nanoparticles and microspheres for the encapsulation of natural antioxidants extracted from Ilex paraguariensis. *Carbohydr. Polym.* **2011**, *84*, 803–806. [CrossRef]

13. Singh, A.; Benjakul, S.; Prodpran, T. Ultrasound-assisted extraction of chitosan from squid pen: Molecular characterization and fat binding capacity. *J. Food Sci.* **2019**, *84*, 224–234. [CrossRef] [PubMed]

14. Lee, D.S.; Woo, J.Y.; Ahn, C.B.; Je, J.Y. Chitosan-hydroxycinnamic acid conjugates: Preparation, antioxidant and antimicrobial activity. *Food Chem.* **2014**, *148*, 97–104. [CrossRef]

15. Muanprasat, C.; Chatsudthipong, V. Chitosan oligosaccharide: Biological activities and potential therapeutic applications. *Pharmacol. Ther.* **2017**, *170*, 80–97. [CrossRef]

16. Ding, L.; Huang, Y.; Cai, X.X.; Wang, S. Impact of pH, ionic strength and chitosan charge density on chitosan/casein complexation and phase behavior. *Carbohydr. Polym.* **2019**, *208*, 133–141. [CrossRef]

17. Koutsopoulou, E.; Koutselas, I.; Christidis, G.E.; Papagiannopoulos, A.; Marantos, I. Effect of layer charge and charge distribution on the formation of chitosan—Smectite bionanocomposites. *Appl. Clay Sci.* **2020**, *190*, 105583. [CrossRef]

18. Luo, X.J.; Peng, J.; Li, Y.J. Recent advances in the study on capsaicinoids and capsinoids. *Eur. J. Pharmacol.* **2011**, *650*, 1–7. [CrossRef]

19. Sukmark, T.; Rachtanapun, P.; Rachtanapun, C. Antimicrobial activity of oligomer and polymer chitosan from different sources against foodborne pathogenic bacteria. *Kasetsart J. Nat. Sci.* **2011**, *45*, 636–643.

20. Benhabiles, M.S.; Salah, R.; Lounici, H.; Drouiche, N.; Goosen, M.F.A.; Mameri, N. Antibacterial activity of chitin, chitosan and its oligomers prepared from shrimp shell waste. *Food Hydrocoll.* **2012**, *29*, 48–56. [CrossRef]

21. Coutinho, T.C.; Ferreira, M.C.; Rosa, L.H.; de Oliveira, A.M.; de Oliveira, J.E.N. *Penicillium citrinum* and *Penicillium mallochii*: New phytopathogens of orange fruit and their control using chitosan. *Carbohydr. Polym.* **2020**, *234*, 1–3. [CrossRef]

22. Vanti, G.L.; Masaphy, S.; Kurjogi, M.; Chakrasali, S.; Nargund, V.B. Synthesis and application of chitosan-copper nanoparticles on damping off causing plant pathogenic fungi. *Int. J. Biol. Macromol.* **2020**, *156*, 1387–1395. [CrossRef]

23. Kamoun, S.; Furzer, O.; Jones, J.D.; Judelson, H.S.; Ali, G.S.; Dalio, R.J.; Roy, S.G.; Schena, L.; Zambounis, A.; Panabières, F.; et al. The top 10 oomycete pathogens in molecular plant pathology. *Mol. Plant Pathol.* **2015**, *16*, 413–434. [CrossRef]

24. Li, N.; Zhou, Q.; Chang, K.F.; Yu, H.; Hwang, S.F.; Conner, R.L.; Strelkov, S.E.; McLaren, D.L.; Turnbull, G.D. Occurrence, pathogenicity and species identification of Pythium causing root rot of soybean in Alberta and Manitoba, Canada. *Crop Prot.* **2019**, *118*, 36–43. [CrossRef]

25. Zerillo, M.M.; Adhikari, B.N.; Hamilton, J.P.; Buell, C.R.; Lévesque, C.A.; Tisserat, N. Carbohydrate-active enzymes in Pythium and their role in plant cell wall and storage polysaccharide degradation. *PLoS ONE* **2013**, *8*, e72572. [CrossRef]

26. Sotelo-Boyás, M.E.; Bautista-Baños, S.; Correa-Pacheco, Z.N.; Jiménez-Aparicio, A. *Chitosan in the Preservation of Agricultural Commodities Chapter 13—Biological Activity of Chitosan Nanoparticles Against Pathogenic Fungi and Bacteria*; Academic Press: Cambridge, MA, USA, 2020; p. 384.

27. Robles, E.; Salaberria, A.M.; Herrera, R.; Fernandes, S.C.M.; Labidi, J. Self-bonded composite films based on cellulose nanofibers and chitin nanocrystals as antifungal materials. *Carbohydr. Polym.* **2016**, *144*, 41–49. [CrossRef]

28. AOAC. *Official Methods of Analysis of the AOAC*, 7th ed.; Government Printing Office: Washington, DC, USA, 1997.

29. Hirai, A.; Odani, H.; Nakajima, A. Determination of degree of deacetylation of chitosan by ^{1}H NMR spectroscopy. *Polym. Bull.* **1991**, *26*, 87–94. [CrossRef]

30. Baxter, A.; Dillon, M.; Anthony Taylor, K.D.; Roberts, G.A.F. Improved method for i.r. determination of the degree of N-acetylation of chitosan. *Int. J. Biol. Macromol.* **1992**, *14*, 166–169. [CrossRef]

31. Affes, S.; Maalej, H.; Aranaz, I.; Acosta, N.; Heras, Á.; Nasri, M. Enzymatic production of low-Mw chitosan-derivatives: Characterization and biological activities evaluation. *Int. J. Biol. Macromol.* **2020**, *144*, 279–288. [CrossRef]

32. Huang, L.; Bi, S.; Pang, J.; Sun, M.; Feng, C.; Chen, X. Preparation and characterization of chitosan from crab shell (*Portunus trituberculatus*) by NaOH/urea solution freeze-thaw pretreatment procedure. *Int. J. Biol. Macromol.* **2020**, *147*, 931–936. [CrossRef]

33. Trung, T.S.; Van Tan, N.; Van Hoa, N.; Minh, N.C.; Loc, P.T.; Stevens, W.F. Improved method for production of chitin and chitosan from shrimp shells. *Carbohydr. Res.* **2020**, *489*, 107913. [CrossRef]

34. Perentena, L.; González, C.; Celis, B.; Valbuena, A.; Colina, M. Síntesis de bases de Schiff derivadas del quitosano por reacción con p-dimetilaminobenzaldehído y 4-hidroxi-3-metoxibenzaldehido. *Rev. Iberoam. de Polímeros* **2015**, *16*, 1–27.

35. Shin, C.S.; Kim, D.Y.; Shin, W.S. Characterization of chitosan extracted from Mealworm Beetle (*Tenebrio molitor Zophobas morio*) and Rhinoceros Beetle (*Allomyrina dichotoma*) and their antibacterial activities. *Int. J. Biol. Macromol.* **2019**, *125*, 72–77. [CrossRef]

36. Fiamingo, A.; Delezuk, J.A.D.M.; Trombotto, S.; David, L.; Campana-Filho, S.P. Extensively deacetylated high molecular weight chitosan from the multistep ultrasound-assisted deacetylation of beta-chitin. *Ultrason. Sonochem.* **2016**, *32*, 79–85. [CrossRef]

37. Delezuk, J.A.d.M.; Cardoso, M.B.; Domard, A.; Campana-Filho, S.P. Ultrasound-assisted deacetylation of beta-chitin: Influence of processing parameters. *Polym. Int.* **2011**, *60*, 903–909. [CrossRef]

38. Yen, M.T.; Yang, J.H.; Mau, J.L. Physicochemical characterization of chitin and chitosan from crab shells. *Carbohydr. Polym.* **2009**, *75*, 15–21. [CrossRef]

39. Mohammed, M.H.; Williams, P.A.; Tverezovskaya, O. Extraction of chitin from prawn shells and conversion to low molecular mass chitosan. *Food Hydrocoll.* **2013**, *31*, 166–171. [CrossRef]

40. Abdel-Rahman, R.M.; Hrdina, R.; Abdel-Mohsen, A.M.; Fouda, M.M.; Soliman, A.Y.; Mohamed, F.K.; Mohsin, K.; Pinto, T.D. Chitin and chitosan from Brazilian Atlantic Coast: Isolation, characterization and antibacterial activity. *Int. J. Biol. Macromol.* **2015**, *80*, 107–120. [CrossRef]

41. Salas, C.; Thompson, Z.; Bhattarai, N. 15—Electrospun chitosan fibers. *Electrospun Nanofibers* **2017**, 371–398. [CrossRef]

42. He, X.; Li, K.; Xing, R.; Liu, S.; Hu, L.; Li, P. The production of fully deacetylated chitosan by compression method. *Egypt. J. Aquat. Res.* **2016**, *42*, 75–81. [CrossRef]

43. Lavertu, M.; Xia, Z.; Serreqi, A.N.; Berrada, M.; Rodrigues, A.; Wang, D.; Buschmann, M.D.; Gupta, A. A validated ^{1}H NMR method for the determination of the degree of deacetylation of chitosan. *J. Pharm. Biomed. Anal.* **2003**, *32*, 1149–1158. [CrossRef]

44. Brugnerotto, J.; Lizardi, J.; Goycoolea, F.M.; Argüelles-Monal, W.; Desbrieres, J.; Rinaudo, M. An infrared investigation in relation with chitin and chitosan characterization. *Polymer* **2001**, *42*, 3569–3580. [CrossRef]

45. Kucukgulmez, A.; Celik, M.; Yanar, Y.; Sen, D.; Polat, H.; Kadak, A.E. Physicochemical characterization of chitosan extracted from *Metapenaeus stebbingi* shells. *Food Chem.* **2011**, *126*, 1144–1148. [CrossRef]

46. Ravi Kumar, M.N.V. A review of chitin and chitosan applications. *React. Funct. Polym.* **2000**, *46*, 1–27. [CrossRef]

47. Antony, R.; Theodore David, S.; Saravanan, K.; Karuppasamy, K.; Balakumar, S. Synthesis, spectrochemical characterisation and catalytic activity of transition metal complexes derived from Schiff base modified chitosan. *Spectrochim. Acta Part Mol. Biomol. Spectrosc.* **2013**, *103*, 423–430. [CrossRef]

48. Sagheer, F.A.A.; Al-Sughayer, M.A.; Muslim, S.; Elsabee, M.Z. Extraction and characterization of chitin and chitosan from marine sources in Arabian Gulf. *Carbohydr. Polym.* **2009**, *77*, 410–419. [CrossRef]

49. Ben Seghir, B.; Benhamza, M.H. Preparation, optimization and characterization of chitosan polymer from shrimp shells. *J. Food Meas. Charact.* **2017**, *11*, 1137–1147. [CrossRef]

50. Dahmane, E.M.; Taourirte, M.; Eladlani, N.; Rhazi, M. Extraction and characterization of chitin and chitosan from parapenaeus longirostris from moroccan local sources. *Int. J. Polym. Anal. Charact.* **2014**, *19*, 342–351. [CrossRef]

51. Jampafuang, Y.; Tongta, A.; Waiprib, Y. Impact of crystalline structural differences between α-and β-chitosan on their nanoparticle formation. *Polymers* **2019**, *11*, 2010. [CrossRef]

52. Yuan, Y.; Chesnutt, B.M.; Haggard, W.O.; Bumgardner, J.D. Deacetylation of chitosan: Material characterization and in vitro evaluation via albumin adsorption and pre-osteoblastic cell cultures. *Materials* **2011**, *4*, 1399–1416. [CrossRef]

53. Goy, R.C.; Morais, S.T.B.; Assis, O.B.G. Evaluation of the antimicrobial activity of chitosan and its quaternized derivative on *E. coli* and *S. aureus* growth. *Rev. Bras. de Farmacogn.* **2016**, *26*, 122–127. [CrossRef]

54. Younes, I.; Sellimi, S.; Rinaudo, M.; Jellouli, K.; Nasri, M. Influence of acetylation degree and molecular weight of homogeneous chitosans on antibacterial and antifungal activities. *Int. J. Food Microbiol.* **2014**, *185*, 57–63. [CrossRef]

55. Palma-Guerrero, J.; Jansson, H.B.; Salinas, J.; Lopez-Llorca, L.V. Effect of chitosan on hyphal growth and spore germination of plant pathogenic and biocontrol fungi. *J. Appl. Microbiol.* **2008**, *104*, 541–553. [CrossRef]

56. Badawy, M.E.I.; Rabea, E.I. Characterization and antimicrobial activity of water-soluble N-(4-carboxybutyroyl) chitosans against some plant pathogenic bacteria and fungi. *Carbohydr. Polym.* **2012**, *87*, 250–256. [CrossRef]

57. Xu, J.; Zhao, X.; Han, X.; Du, Y. Antifungal activity of oligochitosan against *Phytophthora capsici* and other plant pathogenic fungi in vitro. *Pestic. Biochem. Physiol.* **2007**, *87*, 220–228. [CrossRef]

58. Park, R.D.; Jo, K.J.; Jo, Y.Y.; Jin, Y.L.; Kim, K.Y.; Shim, J.H. Variation of antifungal activities of chitosans on plant pathogens. *J. Microbiol. Biotechnol.* **2002**, *12*, 84–88.

59. Mukhtar Ahmed, K.B.; Khan, M.M.A.; Siddiqui, H.; Jahan, A. Chitosan and its oligosaccharides, a promising option for sustainable crop production-a review. *Carbohydr. Polym.* **2020**, *227*, 115331. [CrossRef]

60. Kumaraswamy, R.V.; Kumari, S.; Choudhary, R.C.; Pal, A.; Raliya, R.; Biswas, P.; Saharan, V. Engineered chitosan based nanomaterials: Bioactivities, mechanisms and perspectives in plant protection and growth. *Int. J. Biol. Macromol.* **2018**, *113*, 494–506. [CrossRef]